Available online at www.sciencedirect.com

ScienceDirect

Geochimica et Cosmochimica Acta 315 (2021) 89–100

Geochimica et Cosmochimica Acta

www.elsevier.com/locate/gca

Acid-base properties of *Synechococcus*-derived organic matter

Logan Swaren [a,*], Daniel S. Alessi [a], George W. Owttrim [b], Kurt O. Konhauser [a]

[a] *Department of Earth & Atmospheric Sciences, University of Alberta, Edmonton, Alberta T6G 2E3, Canada*
[b] *Department of Biological Sciences, University of Alberta, Edmonton, Alberta T6G 2E9, Canada*

Received 4 August 2021; accepted in revised form 1 October 2021; Available online 12 October 2021

Abstract

Marine cyanobacteria play an important role in trace metal cycling in the oceans. However, the influence of bacterial detritus following cell lysis – that includes both particulate organic matter (POM) and dissolved organic matter (DOM) – is less understood. Previous investigations have shown that the ratio of bacterial detritus to living cells increases significantly with ocean depth, indicating that the former plays a central role in trace metal cycling and eventual sequestration in deep marine sediments. Thus, in this study we produced detritus from the mechanical lysis of the common marine cyanobacterium *Synechococcus* sp. PCC 7002 (referred to as cyPOM and cyDOM), and then measured their buffering capacity through proton adsorption and release via potentiometric acid-base titrations. Both cyPOM and cyDOM were best modelled using a 2-site non-electrostatic protonation model. The cyPOM fraction possessed ligands with pK_a values of 5.78 (±0.07) and 9.01 (±0.29) with corresponding site concentrations of 41.8 (±8.15) μmol g^{-1} and 41.2 (±5.28) μmol g^{-1}, while cyDOM had pK_a values of 4.89 (±0.22) and 6.80 (±0.22) and corresponding site concentrations of 42.8 (±14.6) μmol g^{-1} and 37.3 (±16.5) μmol g^{-1}. As a comparison, intact *Synechococcus* cells were previously reported to be best modelled by invoking 3-sites with overall ligand densities more than double that of cyPOM and cyDOM. Trace metal (Cd, Co, Cu, Ni, and Zn) adsorption experiments indicate that cyPOM has a lower affinity towards trace metals than intact *Synechococcus* cells, evidenced by lower trace metals adsorption per gram of dry mass and therefore less trace metal sequestration potential. This implies that intact *Synechococcus* cells are chiefly responsible for trace metal sequestration, even at high cyPOM proportions (10:1 – cyPOM:*Synechococcus*) that are more representative of POM that reaches the seafloor. The cyDOM-trace metal association could not be determined experimentally; thus we applied existing thermodynamic data from modern marine DOM studies acquired via potentiometric titrations and metal-binding constants. Unlike cyPOM, metal speciation is almost entirely accounted for in the dissolved fraction (>99.9%). These results further the view that DOM is the most important microbial fraction in controlling metals speciation in the water column.

Keywords: Cyanobacteria; *Synechococcus*; Particulate organic matter; Bacterial detritus; Surface complexation modelling; Acid-base titration

1. INTRODUCTION

The distributions of a number of trace metals (e.g., cadmium, cobalt, copper, nickel, and zinc) in seawater are closely correlated to marine primary productivity and biological cycling in the water column (Bruland, 1980; Bruland et al., 1991; Sunda and Huntsman, 1995; Morel and Price, 2003; Saito et al., 2003; Sunda, 2012; Bruland et al., 2013; Twining and Baines, 2013). They demonstrate nutrient-type distributions in marine water columns, characterized by a sharp decrease in concentration in surface waters due to assimilation and adsorption by phytoplankton paired with an increase in concentration with depth due to remineralization as a result of respiration (Bruland

* Corresponding author at: 3-11 Earth Sciences Building, University of Alberta, Edmonton, AB T6G 2E3, Canada.
E-mail address: lswaren@ualberta.ca (L. Swaren).

https://doi.org/10.1016/j.gca.2021.10.003
0016-7037/

and Lohan, 2003). The main primary producing phytoplankton in nutrient-rich regions of the oceans are marine cyanobacteria, namely *Prochlorococcus* and *Synechococcus* (Flombaum et al., 2013). *Synechococcus* populations vary from 10^4 to 10^5 cells mL^{-1} within the photic zone in the relatively rich waters of the Arabian Sea and off the coast of Peru (Waterbury et al., 1979; Worden et al., 2004). Populations have been reported up to 10^6 cells mL^{-1} in the Chesapeake Bay during warm summer months. During this time picoplankton primary productivity exceeds that of the heterotrophic bacteria community (Wang et al., 2011).

There are numerous studies that have investigated the ability of phytoplankton to assimilate trace metals (e.g., Ho et al., 2003; Twining and Baines, 2013), but this is outside the focus of this work. Instead, we concentrate here on the adsorptive capacity of cyanobacteria and some of their lysates toward trace metals because past experimental work demonstrated that organic functional groups associated with their cell walls are reactive towards trace metals at seawater pH (e.g., Liu et al., 2015; Bishop et al., 2019; Swaren et al., 2021). Indeed, based on these studies, it has even been suggested that intact cells could conceivably adsorb nearly all the dissolved trace metals from seawater (Bishop et al., 2019). However, in nature the picture is more complicated because intact cells compete for dissolved metals with cell detritus, commonly particulate organic matter (POM) as well as the dissolved organic matter (DOM) pool.

Cyanobacterial cell-derived POM provides one mechanism by which trace metals can be transported to the sea floor (Boeuf et al., 2019; Kharbush et al., 2020). POM is operationally defined as biomass, including phytoplankton, bacterial detritus (composed of dead cells and cell fragments), zooplankton fecal pellets, and various types of aggregates (Le Moigne, 2019; Kharbush et al., 2020). There are two major processes by which cyanobacterial cell detritus is produced: (1) lysis by viral pathogens and (2) zooplankton grazing (Pernthaler, 2005; Kawasaki et al., 2011; Zheng et al., 2019). Related to the latter process is "sloppy feeding", a term attributed to the disaggregation of phytoplankton cells by zooplankton mouthparts resulting in the release of undigested particulates as well as DOM (Strom et al., 1997; Saba et al., 2011). Kawasaki et al. (2011) determined that approximately 15% of POM in the top 300 m of the open ocean in the North Pacific comprised of living cyanobacteria and that about 6% of the POM was composed of cyanobacteria and heterotrophic bacteria detritus. Interestingly, the ratio of cyanobacterial cell detritus to living cells increased with increasing depth, indicating that the lack of sunlight inhibits productivity and phytoplankton cells inevitably degrade as they sink (Kawasaki et al., 2011). For example, in the Southern Ocean, living cyanobacteria can make up 14 to 45% of surface water POM and decrease to as little as 2% at depths greater than 210 m (Tremblay et al., 2015). By contrast cyanobacteria and heterotrophic bacteria detritus made up to a maximum of 41% of deep (>210 m) POM in the same location (Laurenceau et al., 2014; Tremblay et al., 2015).

There is also a growing understanding of the molecular composition of the cyanobacteria-derived DOM pool (e.g., Zhao et al., 2017, 2019; Ma et al., 2018; Zheng et al., 2019). In the modern oceans DOM is a complex mixture of carboxyl-rich, alicyclic molecules (CRAM), humic and fulvic acids, and polysaccharides, representing a bulk pool of terrestrial and marine sources (Hansell and Carlson, 2001; Engel et al., 2004; Pedler-Sherwood et al., 2015; Walker et al., 2016; Fatayer et al., 2018; Jiao et al., 2018). Fulvic acids are the major constituent of organic matter found in rivers and streams (Celo et al., 2001), and lignin oxidation products are commonly employed as biomarkers to identify the influence of terrestrially-derived dissolved organic carbon (DOC) (Opsahl & Benner, 1997; Dilling & Kaiser, 2002; Dittmar et al., 2006). By contrast, marine-derived DOM comprises material from cell lysis but also organic ligands that are generated to either scavenge because of their nutritional requirements or to minimize their toxicity via organic chelation (Zhang et al., 2019).

In the present study we investigate the surface reactivity and trace metal binding behaviour of *Synechococcus* sp. PCC 7002 derived POM and DOM following mechanical lysis to assess how their surface reactivities compare to previous reports of intact cells. We chose *Synechococcus* because of the abundant extant literature on the composition of its cell wall, surface charge variations with pH and its ability to adsorb a number of trace metals from seawater. Therefore, we have a solid basis with which to compare our experimental results. Focusing on the acid-base surface properties and speciation of trace metals between *Synechococcus* and their derived cyanobacterial cell detritus also provides necessary insight to the distribution of trace metals being deposited on the seafloor via intact cells and their lysates.

2. METHODS

2.1. *Synechococcus* sp. PCC 7002 growth

The unicellular cyanobacterium *Synechococcus* sp. PCC 7002 (*Synechococcus*) was cultured on A + medium agar plates, aerobically, at 30 °C under a light intensity of 50 μmol photons m^{-2} s^{-1}. After a suitable colony was established, it was transferred to a 250 mL Erlenmeyer flask containing 50 mL of A + medium using a sterile inoculation loop. The cyanobacterial solution was then gently agitated on an orbital shaker at 60 rpm for 3 days at 30 °C to promote exponential growth and inhibit the settling of cells. The 50 mL solution was then transferred to a 1 L Erlenmeyer flask containing an additional 350 mL of A + media. The 1 L flask was then agitated at 100 rpm for 10 days at 30 °C until the *Synechococcus* achieved stationary growth phase (based on identical growing conditions and OD_{750} measurements previously observed in our laboratory; see Liu et al., 2015). During the 10-day agitation period, the cyanobacterial solution was aerated with 0.2 μm filtered, humidified air directly into the solution.

2.2. *Synechococcus* harvesting

To harvest the *Synechococcus* cells, the bacterial solution was centrifuged (Sorvall Lynx 4000) five times at 10,000*g* for five-minute intervals with 0.56 M NaCl to simulate marine ionic strength, and to remove residual growth media as well as potential competing metals from the cell wall. After each centrifugation, the resulting supernatant was discarded, and the cells were resuspended in 0.56 M NaCl for each wash interval. Following the final wash interval, the wet mass of the resulting *Synechococcus* cell pellet was measured, and then resuspended in 0.56 M NaCl to give a final cell concentration of 10 g L^{-1} as wet weight. No significant cell lysis has previously been recorded using this washing procedure (Fein et al., 1997; Fowle and Fein, 2000; Liu et al., 2015).

2.3. Preparation of mechanically lysed cyPOM and cyDOM

Mechanical lysis, achieved through high pressure homogenization, is commonly used to represent intracellular DOM resulting from cell breaking during sloppy feeding of phytoplankton by grazers such as copepods (Ma et al., 2018). Zheng et al. (2019) used high-pressure and freeze–thaw treatments to produce *Synechococcus*-derived DOM to investigate molecular characteristics of microbial recalcitrant DOM (RDOM) during incubation experiments. Outside the scope of these previous studies is the influence of mechanical lysis, or sloppy feeding, on remnant cell detritus surface reactivity. In this study, mechanical lysis of cyanobacterial cells was accomplished via sonication as it does not introduce chemicals that have the potential to adsorb to the lysed cells (Braun-Sonic, 2000). To do so, 10 mL aliquots of the washed 10 g L^{-1} bacterial cell solution were separated into 15 mL polypropylene tubes prior to sonication. Each tube was sonicated at 160 MHz and 50 W for a duration of 30 s and then immediately inserted into an ice-water bath. Samples were cooled between cycles to minimize protein denaturing as a result of the heat produced during sonication. Each aliquot underwent eight cycles of sonication, with breaks after the third and sixth cycle to mix all tubes together into a sterile 250 mL Erlenmeyer flask, after which the suspension was re-distributed into 10 mL aliquots to ensure homogeneity of the resulting *Synechococcus* lysate solution (Bishop, 2018). Cyanobacteria lysis was confirmed by autofluorescence using a Zeiss Axioskop 2 epifluorescence light microscope. The cultured *Synechococcus* displayed near complete autofluorescence (>99%) upon visual inspection whereas lysed cells displayed <5%. The lysed samples were centrifuged for five minutes at 10,000*g* to separate the dissolved and particulate fractions. The resulting supernatant was filtered through 0.2 μm nylon membranes. Hereafter we refer to the filtered lysate as cyDOM. The resulting wet pellet was weighed and resuspended to 10 g L^{-1} in 0.56 M NaCl. The resulting lysed solution was considered an analog for marine particulate organic matter, herein referred to as cyPOM.

2.4. Attenuated total reflectance Fourier transform infrared (ATR-FTIR) spectroscopy

After cyPOM resuspension in 0.56 M NaCl, the 10 g L^{-1} solution was filtered through 0.2 μm nylon membranes. The filter was then rinsed with ultrapure water to minimize salt precipitation. The cyPOM was then removed from the nylon membrane using ultrapure water and then oven dried for 24 h at 50 °C. Once dried, samples were crushed using an agate mortar and pestle to produce a powder. Intact *Synechococcus* cells were prepared in the same manner to compare the effect of mechanical lysis. The dried cyPOM was then analyzed by attenuated total reflectance Fourier transform infrared (ATR-FTIR) spectroscopy (Bruker Platinum ATR). The spectra were recorded as 16 co-added interferograms at a resolution of 4 cm^{-1}. Baseline correction of the spectra was done using the OPUS software interface (Version 7.2).

2.5. Zeta potential

Following cell washing and lysis, the 10 g L^{-1} cyPOM suspension was diluted to 0.2 g L^{-1} in sterile 15 mL polypropylene tubes. The pH of each tube was adjusted to cover a range of 3–9 using small aliquots of 0.1 and 1 M HNO_3 and NaOH. Samples were placed on an end-over-end rotator at 30 rpm between pH adjustments. Samples were rotated for a minimum of 1 hr in between additions of acid or base and then left overnight to ensure equilibrium had been achieved prior to measuring the final solution pH values. Zeta potential measurements were conducted with a Zetasizer Nano Series instrument (Malvern Instruments, United Kingdom). The average of 3 separate cyPOM batches are reported. Each sample was measured 3 times with a minimum of 10 readings per measurement.

2.6. Potentiometric titrations

Acid-base titrations were performed on 50 mL of the cyPOM suspension diluted 1:9 (v:v) with 0.56 M NaCl to yield a concentration of 0.14 g L^{-1} (dry mass – 7:50 [dry:wet]) and 50 mL of the cyDOM diluted 1:1 (v:v) with 0.56 M NaCl, using a Metrohm Titrando 905 autotitrator. Prior to titration, the pH probe was calibrated using commercially available pH buffers (Fischer Scientific; pH 4.0, 7.0, and 10.0). The lysate was isolated from the atmosphere and purged 30 min before and during the titration with N_2 gas. Following the 30-min N_2 purge, the initial "down" titration was begun by adding 0.1 M HNO_3 to lower the pH to 3. Once the lysate pH reached 3, an "up" titration ensued by the addition of small volumes of 0.1 M NaOH. At pH 10.5, the "up" titration stopped and the subsequent "down" titration commenced through the addition of 0.1 M HNO_3 until a pH of 3 was achieved again. The second "down" titration was conducted to ensure that the cyPOM was not damaged during the process, as indicated by the presence of hysteresis between

the forward and reverse proton buffering curves (Hao et al., 2018). An electrode stability of 0.1 mV s^{-1} was achieved before further additions of acid or base to ensure chemical equilibrium throughout the titration procedure. The titration pH and corresponding volumes of acid and base added were recorded autonomously by the titration software (tiamo 2.5) and processed to find the proton budget. Titration data were modelled by invoking one, two, and three monoprotic reactions using the following reaction stoichiometry:

$$>X^- + H^+ \leftrightarrow >XH \quad (1)$$

where $>X^-$ is the general deprotonated surface functional group and >XH is the corresponding protonated state. The corresponding mass action constant (K) can be defined from Eq. (1) as:

$$K = \frac{[>XH]}{[>X^-] \cdot a_{H^+}} \quad (2)$$

where square brackets represent molar concentrations of surface sites and a_{H+} is the solution proton activity. The processed data were used to develop a protonation model and solve for site concentrations and corresponding pK_a values using the software FITEQL 4.0 (Herbelin & Westall, 1999). Following the titration, the solution was vacuum filtered onto pre-weighted 0.2 μm nylon membranes to determine the dry mass for normalization of modeled surface functional group site densities and to calculate the dry mass in g L^{-1} reported above.

2.7. Trace metal adsorption experiments to cyPOM

Following lysis, cyPOM was re-suspended to 10 g L^{-1} in 0.56 M NaCl spiked with 1 ppm cadmium (Cd), cobalt (Co), copper (Cu), nickel (Ni), or zinc (Zn) in an acid-washed 150 mL beaker. The cyPOM-metal solution was then stirred using a magnetic stir-bar for 10 min to ensure homogeneity. After 10 min, while still being stirred, 10 mL aliquots were pipetted from the cyPOM slurry and transferred to a set of seven 15 mL polypropylene test tubes. The pH of each tube was adjusted as described above. Following the final pH reading, samples were filtered through 0.2 μm nylon membranes, diluted 10 × with 2% HNO_3 and 0.5% HCl solutions and the aqueous trace metal concentrations analyzed via ICP-MS/MS (Agilent 8800 Triple Quadrupole).

3. RESULTS

3.1. Attenuated total reflectance Fourier transform infrared (ATR-FTIR) spectroscopy

The ATR-FTIR spectra and functional group assignments for *Synechococcus* sp. PCC 7002 cells and derived cyPOM cells are summarized in Fig. 1. Differences in the spectra of intact *Synechococcus* cells compared to those of cyPOM were minor and within the analytical error of the technique. The peak spanning broadly from 3500 to 3000 cm^{-1} can be assigned to amino groups overlapping with hydroxyl groups in water (Ozturk et al., 2010; Liu et al., 2015). The peak cluster ranging 3000–2800 cm^{-1} is characteristic of alkanes, indicating the presence of methyl and methylene groups typically found in fatty acid components of phospholipids in membrane components (Jiang et al., 2004; Benning et al., 2004; Yee et al., 2004). The distinct peaks at 1645, and 1535 cm^{-1} indicate the presence of primary and secondary amides, respectively, characteristic of proteins and lipopolysaccharides on the cyanobacterial outer membrane (Jiang et al., 2004; Liu et al., 2015). Both *Synechococcus* cells and cyPOM demonstrate a peak cluster in the 1200–950 cm^{-1} range characteristic of carbohydrates (Bouhedja et al., 1997; Jiang et al., 2004; Liu et al., 2015). Several peaks in the carbohydrate range can be attributed to cyanobacterial cell wall components – such as amino sugars likely derived from phospholipids and peptidoglycan (Bouhedja et al., 1997).

3.2. Zeta potential

The cell surface charge was measured as a function of pH for both *Synechococcus* cells and cyPOM (Fig. 2). Both intact *Synechococcus* and cyPOM exhibit a negative surface charge across the entire tested pH range (3–9). Intact *Synechococcus* remains around −15.0 mV from pH 3 to 9, whereas cyPOM becomes more negatively charged with increasing pH. At pH 3, cyPOM has cell surface charge of −4.0 mV and increases to −12.0 mV at pH 5 after which it remains consistent.

3.3. Potentiometric titrations

Best-fit protonation model results obtained from FITEQL 4.0 (Herbelin and Westall, 1999) and the triplicate titrations data for cyPOM and cyDOM can be found in Tables S1 and S2, respectively. Negligible hysteresis was observed when comparing forward and reverse titrations data, indicating no damage to organic components or precipitation of inorganic phases (Figure S1). Several models, including one-, two-, and three-site non-electrostatic protonation models were tested while fitting the titration data (Figure S2). By visual observation, both the two- and three-site models better fit the titration data than the one-site model. Results for cyPOM were determined to be best simulated by a two-site protonation model, based on the variance (V_y) parameter in FITEQL being closest to 1.0 (Herbelin and Westall, 1999; Table S1). Although the 3-site model V_y values are similar to those of the 2-site models, the 3-site models had higher variability in site concentration values than the 2-site models (Table S1). Thus, the best-fitting non-electrostatic protonation model had two functional groups with pK_a values of 5.78 (±0.07) and 9.01 (±0.29), with corresponding site concentrations of 41.8 (±8.15) μmol g^{-1} and 41.2 (±5.28) μmol g^{-1}, respectively (Table 1).

Both 1- and 2-site non-electrostatic protonation models fit the cyDOM titration data well, with the 2-site model having slightly better V_y values (see modelling results in Table 2 and triplicate data in Table S2). The 2-site non-electrostatic protonation model had functional groups with pK_a values of 4.89 (±0.22) and 6.80 (±0.22), and corresponding site concentrations of 42.8 (±14.6) μmol g^{-1} and 37.3 (±16.5) μmol g^{-1}, respectively (Table 2).

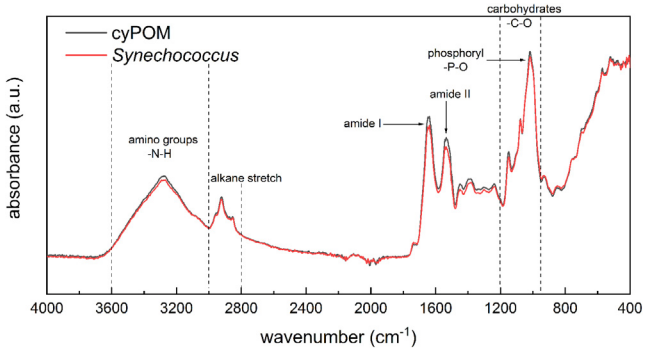

Fig. 1. Attenuated total reflectance fourier transform infrared (ATR-FTIR) spectra of dried and ground Synechococcus sp. PCC 7002 cells overlain with dried and ground cyPOM.

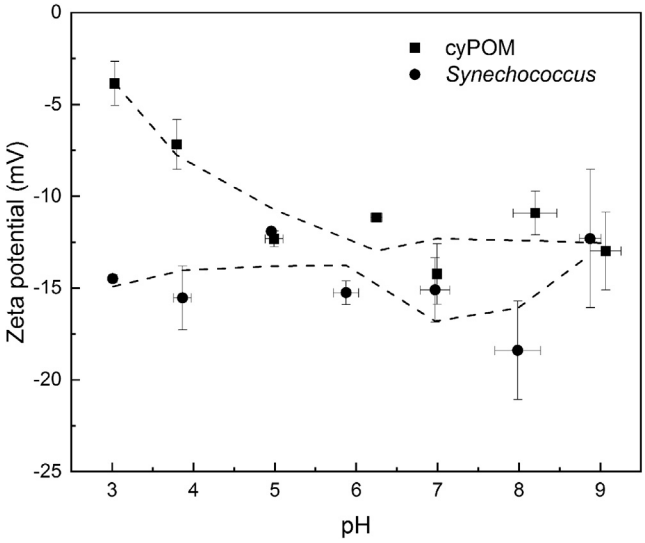

Fig. 2. Zeta potential measurements performed on 0.2 g L^{-1} suspensions of Synechococcus sp. PCC 7002 and cyPOM in 0.56 M NaCl as a function of pH.

Table 1
Summary of protonation modeling of cyPOM in comparison with intact Synechococcus cells from Liu et al. (2015).

Site	pKa	Site Density (mmol g^{-1})	Material	Reference
1	5.78(±0.07)	5.97(±1.16)	cyPOM	This study
	5.07(±0.03)	11.70(±0.62)	Synechococcus cells	Liu et al. (2015)
2	9.01(±0.29)	5.89(±0.75)	cyPOM	This study
	6.71(±0.07)	5.72(±0.22)	Synechococcus cells	Liu et al. (2015)
3	8.54(±0.15)	6.96(±0.76)	Synechococcus cells	Liu et al. (2015)

3.4. Experimental trace metal adsorption to cyPOM

Using the pK_a values and site concentrations determined from the potentiometric titration results, a non-electrostatic (NEM) surface complexation model (SCM) approach was utilized to model the trace metal adsorption data and calculate the trace metal adsorption equilibrium constants to cyPOM (K values). This was achieved by allowing the trace metal of interest (M^{m+}) to sorb to the two proton-active functional groups, using reactions (2) and (3):

$$>L_1\text{-}+M^{m+} \leftrightarrow >L_1\text{-}M^{(m-1)+} \quad (3)$$

$$>L_2\text{-}+M^{m+} \leftrightarrow >L_2\text{-}M^{(m-1)+} \quad (4)$$

where $>L\text{-}O^-$ is the generalized deprotonated surface functional group and $>L\text{-}M^{(m-1)+}$ is the corresponding adsorbed trace metal–ligand complex. Aqueous complexation constants for the trace metals under investigation that were used in FITEQL 4.0 (Herbelin and Westall, 1999) are given in Table S3. The corresponding mass action constants (K) can be defined from Eqs. (3) and (4) as:

$$K1 = \frac{\left[>L_1 - M^{(m-1)+}\right]}{\left[>L_1^-\right] \cdot a_{M^{m+}}} \quad (5)$$

Table 2
Best fit, 2- and 1-site protonation models for cyDOM in comparison with values compiled from literature. Site concentrations are in units of μmol g^{-1}.

pKa 1	Site Conc.	pKa 2	Site Conc.	Material/Sample Location	Reference
4.89(±0.22)	42.8(±14.6)	6.80(±0.22)	37.3(±16.5)	cyDOM	This study
3.42(±0.03)	13.7(±0.27)[a]	–	–	Narragansett Bay DOM	Huizenga and Kester (1979)
3.67(±0.02)	10.3(±0.13)[a]	–	–	Mixed river water DOM	
3.56(±0.02)	10.0(±0.16)[a]	–	–	Block Island Sound DOM (surface)	
3.56(±0.03)	11.6(±0.28)[a]	–	–	Sargasso Sea DOM	
3.75(±0.03)	9.6(±0.25)[a]	–	–	Equatorial Atlantic DOM	
3.61(±0.03)	9.7(±0.21)[a]	–	–	Coastal Equatorial Atlantic DOM (surface)	
3.57(±0.04)	10.9(±0.31)[a]	–	–	Equatorial Atlantic DOM (surface)	
3.67(±0.02)	9.0(±0.12)[a]	–	–	Coastal Peru (low productivity)	
2.66(±0.10)	2.49(±0.07)[b]	4.21(±0.08)	1.70(±0.05)[b]	Aquatic Fulvic Acid	Paxeus and Wedborg (1985)[c]
4.46	80.0[d]	6.64	105.0[d]	Satilla River estuarine DOM	Cai et al. (1998)[e]
4.07(±0.12)	–	–	–	Pristine Barataria Bay DOM	Zhang et al. (2013)
4.57(±0.03)	–	–	–	Pristine Barataria Bay DOM	
4.64(±0.05)	–	–	–	Oil-impacted Barataria Bay DOM	
4.31(±0.03)	–	–	–	Oil-impacted Barataria Bay DOM	
4.13(±0.02)	–	–	–	Oil-impacted Barataria Bay DOM	
4.00	–	8.76	–	Simple Organic Acids	Ritchie and Perdue (2008)
3.91	–	10.09	–	Suwannee River Fulvic Acids	
4.28	–	9.90	–	Suwannee River Humic Acids	
3.82	–	10.28	–	Nordic Fulvic Acids	
4.25	–	10.19	–	Nordic Humic Acids	
3.61	–	9.87	–	Soil Fulvic Acids	
3.97	–	9.71	–	Peat Fulvic Acids	
4.18	–	5.33	–	Laurentian River Fulvic Acids	Garnier et al., 2004[f]
4.71	–	5.90	–	Laurentian River Humic Acids	
3.26	–	8.60	–	Baltic fjord seawater (NW Germany)	Lodeiro et al. 2020

[a] Values reported in μmol mg^{-1} org C.
[b] Values reported in mmol g^{-1}.
[c] Paxeus and Wedborg (1985)reported 4 additional pKa values of 5.85, 6.65, 8.11, and 9.54.
[d] Values reported in μmol L^{-1}.
[e] Cai et al. (1998) reported the presence of 2 additional pKa values at 8.94 and ~10.
[f] Garnier et al. (2004) reported the presence of 4 additional pKa values for Laurentian River Fulvic Acids (6.58, 7.61, 8.93, and 9.99) and Laurentian River Humic Acids (6.67, 7.74, 9.2, and 10.08).

$$K2 = \frac{\left[> L_2 - M^{(m-1)+}\right]}{\left[> L_2^-\right] \cdot a_{M^{m+}}} \quad (6)$$

Square brackets represent surface site molar concentrations and a_M^{m+} is the solution activity of the metal (M) of interest. Aqueous SCM fit results are shown with modelled experimental data in Fig. 3, and the corresponding metal adsorption equilibrium constants are given in Table 3. The two chemical systems tested in FITEQL 4.0 and their resulting adsorption equilibrium constants can be found in Table S3. The results provided in Table S4 are based on the FITEQL 4.0 variance parameter, V(y), the accepted values are between $0.1 < V(y) < 20$ with the best fit being closest to 1.0 (Herbelin and Westall, 1999).

For all 5 trace metals tested (Cd, Co, Cu, Ni, and Zn) metal adsorption to cyPOM increased with increasing pH, a well-documented result consistent with the increasingly negative charge of the cyPOM surface as its functional groups deprotonate at higher pH. All trace metals demonstrate minimal adsorption at acidic pH values (<4) with the exception of Cu that has nearly 40% adsorption at pH 3. Following Cu, Zn and Ni are the most readily adsorbed, followed by Co and Cd in the order Cd < Co < Ni < Zn < Cu. Best-fit metal binding constants for the two proton-active functional groups on cyPOM appear in Table 3.

4. DISCUSSION

4.1. Comparison of cyPOM and cyanobacterial cell surface reactivities

Previous investigations of *Synechococcus* sp. PCC 7002 using potentiometric titrations found that live cells were best modeled using a non-electrostatic 3-site protonation model (Liu et al., 2015), with pK_a values of 5.07, 6.71, and 8.54, inferred to correspond to carboxyl, phosphoryl, and amino surface functional groups, respectively. Following mechanical lysis via sonication, cyPOM investigated in this study was better fit using a 2-site protonation model with pK_a values of 5.78 and 9.01. The pK_a value 5.78 likely corresponds to a mixture of carboxyl and phosphoryl groups. The pK_a value of 9.01 is more likely a combination of various groups such as amino and hydroxyl. Small thiol-bearing molecules also have pK_a values that range from 8-10, as well as recently identified sulfhydryl groups (9.2–9.4) (Yu et al., 2014).

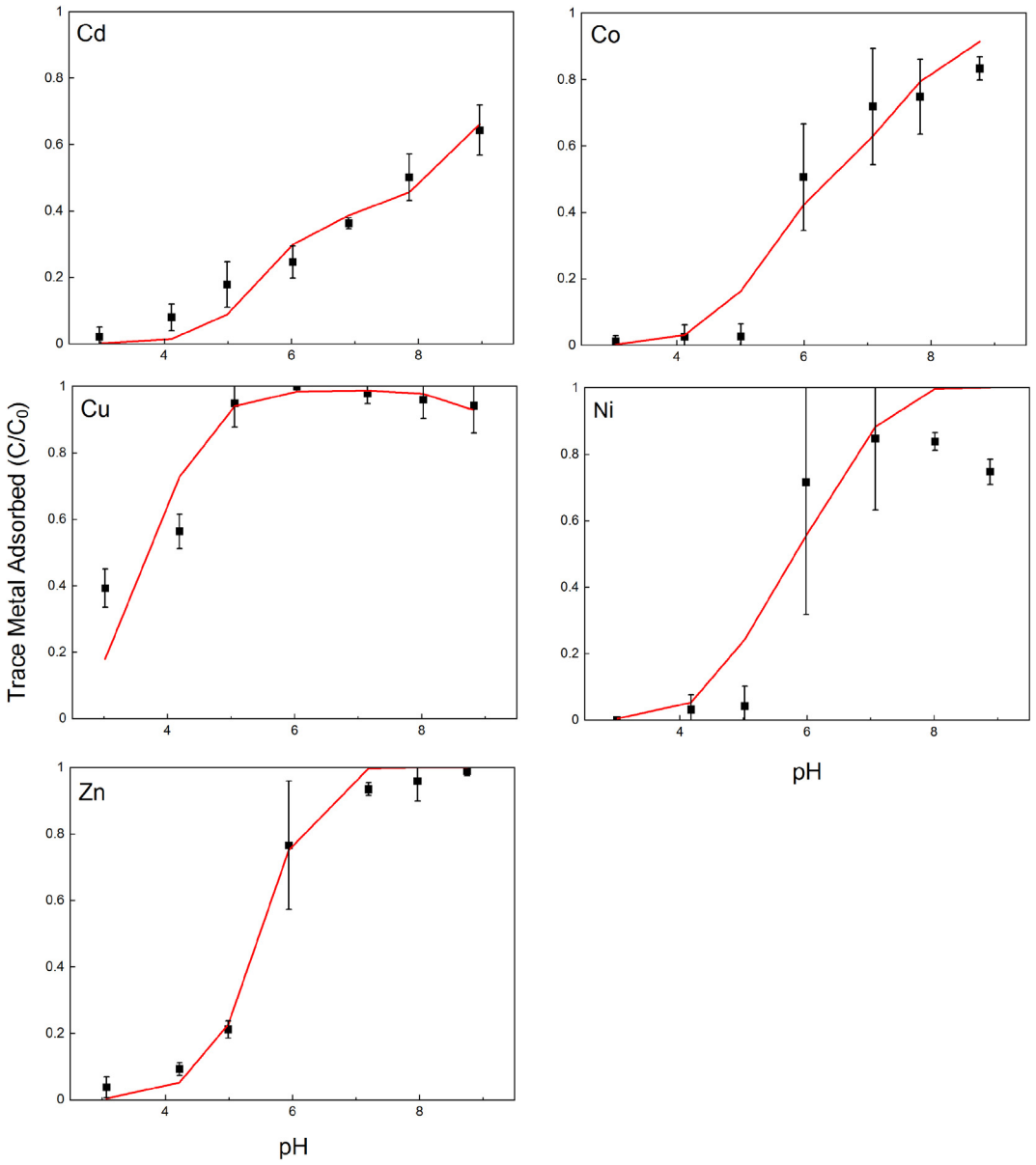

Fig. 3. Modeling (red lines) and experimental (points) results of trace metal adsorption onto 10 g L^{-1} Synechococcus sp. PCC 7002 derived cyPOM in 0.56 M NaCl. Error bars indicate 1-sigma standard deviation. (For interpretation of the references to colour in this figure legend, the reader is referred to the web version of this article.)

Table 3
Best fit binding constants for trace metal-cyPOM complexes and previously studied trace metal-*Synechococcus* sp. PCC 7002 complexes. All experiments were conducted in 0.56 M NaCl.

Trace Metal	Site 1 logK	Site 2 logK	Site 3 logK	Material	Reference
Cd	1.6	1.1	–	cyPOM	This study
	1.15	1.78	2.74	*Synechococcus cells*	Liu et al. (2015)
Co	1.2	2.8	–	cyPOM	This study
	4.6	6.3	–	*Synechococcus cells*	Bishop et al., 2019
Cu	0.7	6.3	–	cyPOM	This study
	3.7	7.4	–	*Synechococcus cells*	Bishop et al., 2019
Ni	0.8	3.7	–	cyPOM	This study
	4.7	6.1	–	*Synechococcus cells*	Bishop et al., 2019
Zn	1.1	2.7	–	cyPOM	This study
	4.4	7.9	–	*Synechococcus cells*	Bishop et al., 2019

As the relative abundance of cyanobacteria and heterotrophic bacteria detritus increases with water column depth, the portion of POM released or exposed during sloppy feeding becomes more refractory as the labile portions are remineralized (Kawasaki et al., 2011). This relatively fresh portion of phytoplankton intracellular components demonstrate a lower overall site density (11.8 mmol g^{-1}) compared to that of intact cells (24.3 mmol g^{-1}; Liu et al., 2015). The ATR-FTIR spectra of both intact cells and cyPOM were nearly identical, indicating that there were not measurable bonding environment differences between dried cells and bacterial detritus caused by mechanical lysis (Fig. 1). Interestingly, the zeta potential of intact *Synechococcus* cells was more negative than cyPOM at more acidic pH, pH < 6 (Fig. 1), indicating that mechanical lysis influenced the cell surface charge, but not the bonding environments. This is likely due to changes in cell surface physiology following cell breakage resulting in surface charge changes, as well as the interaction of surface functional groups carrying a more positive charge with solution that were not in contact with solution prior to cell lysis. This change in surface functional group distribution is exhibited by the expression of surface functional group pK_a values in our protonation model. This alteration is likely not detected by ATR-FTIR as the method probes the cell as a whole and not simply the cell surface (Kenney and Gorzsas, 2019).

4.2. Differences in trace metal affinities between intact cells and cyPOM

The metal-binding constants for Cd identified for cyPOM were similar to values identified by Liu et al. (2015) for *Synechococcus* cells (1.6 and 1.1 versus 1.2, 1.8, and 2.7 for *Synechococcus*). Bishop et al. (2019) found that the metal-binding constants for *Synechococcus* were approximately 4 × greater for site 1 and a minimum of 2 × greater for site 2 than cyPOM (Table 3), the exception being the log K_{Cu} value for the second site (6.3 for cyPOM versus 7.4 for intact *Synechococcus* cells). Our study and modern oceanographic investigations show that cyanobacteria and heterotrophic bacteria detritus is likely more representative of organic matter deposited in deep ocean sediments, meaning that previous estimates of trace metal sequestration based on the surface reactivity of intact phytoplankton are likely overestimated given the higher trace metal affinities to living cells.

Using the calculated pKa values, corresponding site concentrations, and metal binding constants from our thermodynamic modelling, combined with complimentary published *Synechococcus* cell data from our lab (Bishop et al., 2019), we ran predictive models using FITEQL 4.0 (Herbelin and Westall, 1999) to investigate the speciation of the trace metals in the presence of both intact *Synechococcus* and cyPOM. In the presence of both 1 g L^{-1} *Synechococcus* and cyPOM, nearly all metal adsorption (>99.9%) is to *Synechococcus* at pH values above 7. Additionally, to account for the changing proportions of bacterial detritus versus intact cyanobacterial cells in the deep ocean, we modelled a system containing 0.1 g L^{-1} *Synechococcus* and 1 g L^{-1} cyPOM and found the same distribution; that trace metals demonstrated a profoundly higher propensity to adsorb to the surface of the cyanobacterial cells than to cyPOM.

4.3. Surface reactivity of seawater cyDOM

Previous investigations of natural DOM yielded a large array of pK_a values, hinting to the complexity of ligands occurring naturally in seawater (Table 2). In this study, the *Synechococcus*-derived cyDOM potentiometric titration data were fit with a 2-site model (Table 2). The cyDOM has pK_a values of 4.89 and 6.80 when modelled with a 2-site approach, indicating the presence of carboxyl functional groups with pK_a values commonly ranging from 3-6. As observed in Table 2, carboxyl groups are the most common proton active functional groups found in the environment. A large portion of the global DOM pool is composed of carboxyl-rich alicyclic molecules (CRAM) that can be of both terrestrial, with which they are commonly grouped, or marine microbial communities (Hansell, 2013; Lechtenfeld et al., 2014). The second site in the 2-site model has a pKa value of 6.80, inferred to correspond to a combination of amine and phosphoryl functional groups (Table 2). Site 2 and the site identified in the 1-site model with a value of 6.48 likely correspond to the more complex N, P, and S containing biomolecules released from the cyanobacteria, such as amino and nucleic acids, proteins, nucleotides, and vitamins (Moran et al., 2016).

Previous studies have identified the presence of proton active functional groups in natural DOM from aqueous environments with pKa values closely resembling those found in cyDOM, 4.89 and 6.80 (Paxeus and Wedborg, 1985; Cai et al., 1998; Garnier et al., 2004). For instance, Cai et al. (1998) investigated the acid-base properties of DOM collected from the Satilla River estuary in Georgia, USA. They identified 4 possible proton active sites in the estuary, with pK_a values of 4.46, 6.64, 8.94, and 10. The higher pK_a values, greater than 10, are indicative of phenolic hydroxyl groups that represent the presence of terrestrial DOM with a high degree of aromaticity (Koch et al., 2005). Similar measurements were made by Garnier et al., 2004 who identified pK_a values of ~10 in both Laurentian River fulvic and humic acids. Ritchie and Perdue (2008) found that various humic and fulvic acids of terrestrial origin were best modelled by 2-sites with pKa values of <4.5 and >8.7 hinting to the presence of CRAM and aromatic molecules. Moreover, Huizenga & Kester (1979) analyzed multiple oceanic and estuarine DOM and found only one site with a pKa of <3.8. However, their titration procedure did not include pH values above 7. Future oceanographic investigations of open ocean marine DOM should incorporate acid-base titrations to aid in the comparison with microbial-derived DOM. Current literature is commonly focused on riverine and estuarine DOM that has a large terrestrial input.

4.4. Trace metal interactions with marine DOM

Various marine organisms, including *Synechococcus* (Boiteau and Repeta, 2015), produce metal-chelating

ligands. Some ligands make metals bioavailable, such as siderophores. These are iron (Fe)-specific binding ligands that are excreted by numerous microbial cells to dramatically increase the solubility of Fe(III) and make it amenable to assimilation (Vraspir and Butler, 2009). Other ligands are produced and released extracellularly to immobilize toxic metals, such as Cu and Cd (Bruland et al., 1991). The production of these organic ligands is of global significance in terms of trace metal cycling, with estimates suggesting, for example, that 99.0% of marine Fe(III) is associated with siderophores, while 99.7% of Cu in the northeast Pacific is organically complexed (Coale and Bruland, 1988). Other metals are complexed to a lesser extent, with only 30–50% of Ni being associated with organic ligands (Boiteau et al., 2016). The generally high percentage of metals organically bound versus in ionic form (e.g., Cu^{2+}) means that marine plankton, and the organic ligands that they generate, directly control trace metals speciation and cycling in modern oceans.

Although the abundance and composition of metal-specific marine ligands is well documented (e.g., Fe, Co, Cu, Ni and Zn), little attention has been paid to the role of specific DOM contributions of modern plankton to the overall organic ligand pool. Quantifying the organic complexation of trace metals with *Synechococcus*-derived DOM is analytically difficult given the size range of DOM as well as the unique optimization required for each individual trace metal. For instance, the hydrated radius of the trace metals used commonly overlap with that of DOM inhibiting analysis in the same way as cyPOM (e.g., filtration and quantification via ICP-MS) unreliable (Nightingale Jr., 1959). Moreover, Zn has been identified using both differential pulse anodic stripping voltammetry (DPASV) and competitive ligand exchange cathodic stripping voltammetry (CLE-CSV) (Lohan et al., 2005), whereas Ni is commonly only quantified using CLE-CSV (Van den Berg and Nimmo, 1987; Boiteau et al., 2016). The voltammetry procedure is sensitive to the properties of the DOM and requires careful selection and optimization of the electrode, solution ionic strength, voltage range, metal concentrations, and the competitive ligand (Padan et al., 2021).

Building on our predictive model above, we created models consisting of equal site concentrations of *Synechococcus*, cyPOM, and cyDOM site densities using FITEQL 4.0 (Herbelin and Westall, 1999). Because of the difficulties in determining metal binding constants for DOM, we used the average of compiled modern oceanographic studies (Table S5) for cyDOM, values from this study for cyPOM (Tables 1 and 3), and values previously identified from our lab for *Synechococcus* cells (Liu et al., 2015; Bishop et al., 2019). When previous studies identified only one metal binding constant (e.g., Cd, Co, Ni, and Zn – See Table S5), the 1-site non-electrostatic protonation model pK_a value was used. The predictive models indicate that in systems containing equal amounts of all three components (intact cells, cyPOM, and cyDOM) metal speciation is almost entirely cyDOM bound (>99.9%). This is in agreement with similar Cu predictive modelling done by Bishop et al. (2019) including *Synechococcus* cells and published DOM values. The same holds true for a site concentrations ratio of 1:10:100 (cyDOM:*Synechococcus*:cyPOM) demonstrating the high affinity of trace metals to bind to cyDOM.

Although previous studies have predicted that intact cells can be important sorbents for trace metals (e.g., Konhauser et al., 2018; Bishop et al., 2019), the DOM – although yet to be tested experimentally – appears to be the most important fraction controlling metal speciation. Further studies analyzing trace metal availability in seawater should determine the source of metal-binding ligands, whether that be marine or terrestrial. Progression in high resolution mass spectroscopy (e.g., Fourier transform ion cyclotron resonance mass spectroscopy; FTICR-MS) is beginning to unravel the distinct molecular characteristics and chemical signatures of DOM from various sources (e.g., Ma et al., 2018; Niu et al., 2018). Moreover, researchers are beginning to identify individual metal-binding ligands from DOM samples (e.g., Boiteau et al., 2016; Chen et al., 2017) which will be the motivation of future studies in our lab.

5. CONCLUSIONS

In modern oceans, the majority of phytoplankton biomass deposited in deep ocean sediments is in the form of bacterial detritus rather than living cells. We present here an experimental study coupled to thermodynamic proton and metal binding modelling that indicates that almost all (>99.9%) of the trace metals Cd, Co, Cu, Ni, and Zn would be sorbed to cyanobacterial cells over cyPOM. Although only a small portion of modern POM that reaches the seafloor consists of intact cyanobacterial cells compared to bacterial detritus, that portion would be responsible for the deposition and eventual burial of the trace metals present. Moreover, even in the presence of 1:100 (cyDOM:cyPOM), our predictive models indicate that the metal speciation is almost entirely in the dissolved fraction (>99.9%), comparable to that of many modern marine speciation investigations. These findings further the notion that there is a clear need to better integrate DOM into trace metal speciation in both modern and ancient oceans.

Declaration of Competing Interest

The authors declare that they have no known competing financial interests or personal relationships that could have appeared to influence the work reported in this paper.

ACKNOWLEDGEMENTS

This work was supported by NSERC Discovery Grants to KOK (RGPIN-165831), DSA (RGPIN-04134) and GWO (RGPIN-171319). We would like to thank Dr. Hailiang Dong and three anonymous reviewers whose comments greatly improved this manuscript

APPENDIX A. SUPPLEMENTARY MATERIAL

Supplementary data to this article can be found online at https://doi.org/10.1016/j.gca.2021.10.003.

REFERENCES

Benning L. G., Phoenix V., Yee N. and Konhauser K. O. (2004) The dynamics of cyanobacterial silicification: An infrared micro-spectroscopic investigation. *Geochim. Cosmochim. Acta* **68**, 743–757.

Bishop B. A. (2018) The effects of cyanobacteria and dissolved organic carbon on marine trace metal cycling. *Thesis - Master of Science, University of Alberta*.

Bishop B. A., Flynn S. L., Warchola T. J., Alam M. S., Robbins L. J., Liu Y, Owttrim G. W., Alessi D. S. and Konhauser K. O. (2019) Adsorption of biologically critical trace elements to the marine cyanobacterium *Synechococcus* sp. PCC 7002: Implications for marine trace metal cycling. *Chem. Geol.* **525**, 28–36.

Boeuf D., Edwards B. R., Eppley J. M., Hu S. K., Poff K. E., Romano A. E., Caron D. A., Karl D. M. and DeLong E. F. (2019) Biological composition and microbial dynamics of sinking particulate organic matter at abyssal depths in the oligotrophic open ocean. *Proc. Natl. Acad. Sci.* **116**, 11824–11832.

Boiteau R. M. and Repeta D. J. (2015) An extended siderophore suite from *Synechococcus* sp. PCC 7002 revealed by LC-ICPMS-ESIMS. *Metallomics* **7**, 877.

Boiteau R. M., Till C. P., Ruacho A., Bundy R. M., Hawco N. J., McKenna A. M., Barbeau K. A., Bruland K. W., Saito M. A. and Repeta D. J. (2016) Structural Characterization of Natural Nickel and Copper Binding Ligands along the US GEOTRACES Eastern Pacific Zonal Transect. *Front. Mar. Sci.* **3**, 243.

Bouhedja W., Sockalingum G. D., Pina P., Bloy C., Labia R., Millot J. M. and Manfait M. (1997) ATR-FTIR spectroscopic investigation of *E. coli* transconjugants beta-lactams-resistance phenotype. *FEBS Lett.* **412**, 39–42.

Bruland K. W. (1980) Oceanographic distributions of cadmium, zinc, nickel, and copper in the North Pacific. *Earth Planet. Sci. Lett.* **47**, 176–198.

Bruland K. W., Donat J. R. and Hutchins D. A. (1991) Interactive influences of bioactive trace metals on biological production in oceanic waters. *Limnol. Oceanogr.* **36**, 1555–1577.

Bruland K. W. and Lohan M. C. (2003) Controls of trace metals in seawater. *Treatise Geochem.* **6**, 23–47.

Bruland K. W., Middag R. and Lohan M. C. (2013) Controls of Trace Metals in Seawater. In *Treatise on Geochemistry*, pp. 19–51.

Cai W., Wang Y. and Hodson R. E. (1998) Acid-base properties of dissolved organic matter in the estuarine waters of Georgia, USA. *Geochim. Cosmochim. Acta* **62**, 473–483.

Celo V., Murimboh J., Salam M. S. A. and Chakrabarti C. L. (2001) A kinetic study of nickel complexation in model systems by adsorptive cathodic stripping voltammetry. *Environ. Sci. Technol.* **35**, 1084–1089.

Chen H, Johnston R. C., Mann B. F., Chu R. K., Tolic N, Parks J. M. and Gu B. (2017) Identification of mercury and dissolved organic matter complexes using ultrahigh resolution mass spectrometry. *Environ. Sci. Tech. Lett.* **4**, 59–65.

Coale K. H. and Bruland K. W. (1988) Copper complexation in the Northeast Pacific. *Limnol. Ocean.* **33**, 1084–1101.

Dilling J. and Kaiser K. (2002) Estimation of the hydrophobic fraction of dissolved organic matter in water samples using UV photometry. *Water Res.* **36**, 5037–5044.

Dittmar T., Hertkorn N., Kattner G. and Lara R. J. (2006) Mangroves, a major source of dissolved organic carbon to the oceans. *Global Biogeochem. Cycles* **20**, GB1012. 7 p.

Engel A., Thoms S., Riebesell U., Rochelle-Newall E. and Zondervan I. (2004) Polysaccharide aggregation as a potential sink of marine dissolved organic carbon. *Lett. Nature* **428**, 929–932.

Fatayer S., Coppola A. I., Schulz F., Walker B. D., Broek T. A., Meyer G., Druffel E. R. M., McCarthy M. and Gross L. (2018) Direct visualization of individual aromatic compound structures in low molecular weight marine dissolved organic carbon. *Geophys. Res. Lett.* **45**, 5590–5598.

Fein J. B., Daughney C. J., Yee N. and Davis T. A. (1997) A chemical equilibrium model for metal adsorption onto bacterial surfaces. *Geochim. Cosmochim. Acta* **61**, 3319–3328.

Flombaum P., Gallegos J. L., Gordillo R. A., Rincon J., Zabala L. L., Jiao N., Karl D. M., Li W. K. W., Lomas M. W., Veneziano D., Vera C. S., Vrugt J. A. and Martiny A. C. (2013) Present and future global distributions of the marine Cyanobacteria *Prochlorococcus* and *Synechococcus*. *Proc. Natl. Acad. Sci.* **24**, 9824–9829.

Fowle D. and Fein J. B. (2000) Experimental measurements of the reversibility of metal-bacteria adsorption reactions. *Chem. Geol.* **168**, 27–36.

Garnier C., Mounier S. and Benaim J. (2004) Influence of dissolved organic carbon content on modelling natural organic matter acid-base properties. *Water Res.* **38**, 3685–3692.

Hansell D. A. and Carlson C. A. (2001) Marine dissolved organic matter and the carbon cycle. *Oceanography* **14**, 41–49.

Hansell D. A. (2013) Recalcitrant dissolved organic carbon fractions. *Annu. Rev. Mar. Sci.* **5**, 421–445.

Hao W., Flynn S. L., Alessi D. S. and Konhauser K. O. (2018) Change of point of zero net proton charge (pHPZNPC) of clay minerals with ionic strength. *Chem. Geol.* **493**, 458–467.

Herbelin A. L. and Westall J. C. (1999). FITEQL: a Computer Program for Determination of Equilibrium Constants from Experimental Data. Department of Chemistry, Oregon State University. Corvallis, OR. *Report 99-01*.

Ho T.-Y., Quigg A., Finkel Z. V., Milligan A. J., Wyman K., Falkowski P. G. and Morel F. M. M. (2003) The elemental composition of some marine phytoplankton. *J. Phycol.* **39**, 1145–1159.

Huizenga D. L. and Kester D. R. (1979) Protonation equilibria of marine dissolved organic matter. *Limnol. Oceanogr.* **24**, 145–150.

Jiang W., Saxena A., Song B., Ward B. B., Beveridge T. J. and Myneni S. C. B. (2004) Elucidation of functional groups on gram-positive and gram-negative bacterial surfaces using infrared spectroscopy. *Langmuir* **20**, 11433–11442.

Jiao N., Cai R., Zheng Q., Tang K., Liu J., Jiao F., Wallace D., Chen F., Li C., Amann R., Benner R. and Azam F. (2018) Unveiling the enigma of refractory carbon in the ocean. *Natl. Sci. Rev.* **5**, 459–463.

Kawasaki N., Sohrin R., Ogawa H., Nagata T. and Benner R. (2011) Bacterial carbon content and the living and detrital bacterial contributions to suspended particulate organic carbon in the North Pacific Ocean. *Aquat. Microb. Ecol.* **62**, 165–176.

Kenney J. P. L. and Gorzsas A. (2019) Applications of Fourier-transform Ifrared Spectroscopy in Geomicrobiology. In *Analytical Geomicrobiology: A Handbook of Instrumental Techniques* (eds. J. P. L. Kenney, H. Veeramani and D. S. Alessi). Cambridge University Press, Cambridge, United Kingdom, pp. 79–92.

Kharbush J. J., Close H. G., Van Mooy B. A. S., Arnosti C., Smittenberg R. H., Le Moigne F. A. C., Mollenhauer G., Scholz-Bottcher B., Obreht I., Koch B. P., Becker K. W., Iverson M. H. and Mohr W. (2020) Particulate organic carbon deconstructed: molecular and chemical composition of particulate organic carbon in the ocean. *Front. Mar. Sci.* **7**, 518.

Koch B. P., Witt M., Engbrodt R., Dittmar T. and Kattner G. (2005) Molecular formulae of marine and terrigenous dissolved organic matter detected by electrospray ionization Fourier transform ion cyclotron resonance mass spectrometry. *Geochem. Cosmochim. Acta* **69**, 3299–3308.

Konhauser K. O., Robbins L. J., Alessi D. S., Flynn S. L., Gingras M. K., Martinez R. E., Kappler A., Swanner E. D., Li Y. L., Crowe S. A., Planavsky N. J., Reinhard C. T. and Lalonde S. V. (2018) Phytoplankton contributions to the trace-element composition of Precambrian banded iron formations. *GSA Bulletin* **130**, 941–951.

Laurenceau E. C., Trull T. W., Davies D. M., Bray S. G., Doran J., Planchon F., Carlotti F., Jouandet M. P., Cavagna A. J., Waite A. M. and Blain S. (2014) The relative importance of phytoplankton aggregates and zooplankton fecal pellets to carbon export: insights from free-drifting sediment trap deployments in naturally iron-fertilised waters near the Kerguelen plateau. *Biogeosciences* **11**, 13623–13673.

Lechtenfeld O. J., Kattner G., Flerus R., McCallister S. L., Schmitt-Kopplin P. and Koch B. P. (2014) Molecular transformation and degradation of refractory dissolved organic matter in the Atlantic and Southern Ocean. *Geochem. Cosmochim. Acta* **126**, 321–337.

Le Moigne F. A. C. (2019) Pathways of organic carbon downward transport by the oceanic biological carbon pump. *Front. Mar. Sci.* **6**, 634.

Liu Y., Alessi D. S., Owttrim G. W., Petrash D. A., Mloszewska A. M., Lalonde S. V., Martinez R. E., Zhou Q. and Konhauser K. O. (2015) Cell surface reactivity of *Synechococcus* sp. PCC 7002: implications for metal sorption from seawater. *Geochim. Cosmochim. Acta* **169**, 30–44.

Lodeiro P., Rey-Castro C., David C., Achterberg E. P., Puy J. and Gledhill M. (2020) Acid-base properties of dissolved organic matter extracted from the marine environment. *Sci. Total Environ.* **729** 138437.

Lohan M. C., Crawford D. W., Purdie D. A. and Statham P. J. (2005) Iron and zinc enrichments in the northeastern subarctic Pacific: ligand production and zinc availability in response to phytoplankton growth. *Limnol. Oceanogr.* **50**, 1427–1437.

Ma X., Coleman M. L. and Waldbauer J. R. (2018) Distinct molecular signatures in dissolved organic matter produced by viral lysis of marine cyanobacteria. *Environ. Microbiol.* **20**, 3001–3011.

Moran M. A., Kujawinski E. B., Stubbins A., Fatland R., Aluwihare L. I., Buchan A., Crump B. C., Dorrestein P. C., Dyhrman S. T., Hess N. J., Howe B., Longnecker K., Medeiros P. M., Niggemann J., Obernosterer I., Repeta D. J. and Waldbauer J. R. (2016) Deciphering ocean carbon in a changing world. *Proc. Natl. Acad. Sci.* **113**, 3143–3151.

Morel F. M. M. and Price N. M. (2003) The biogeochemical cycles of trace metals in the oceans. *Science* **300**, 944–947.

Nightingale, Jr., E. R. (1959) Phenomenological theory of ion solvation. Effective radii of hydrated ions. *J. Phys. Chem.* **63**, 1381–1387.

Niu X.-Z., Harir M., Schmitt-Kopplin P. and Croue J.-P. (2018) Characterisation of dissolved organic matter using Fourier-transform ion cyclotron resonance mass spectrometry: type-specific unique signatures and implications for reactivity. *Sci. Total Environ.* **644**, 68–76.

Opsahl S. and Benner R. (1997) Distribution and cycling of terrigeneous dissolved organic matter in the ocean. *Nature* **386**, 480–482.

Ozturk S., Aslim B. and Suludere Z. (2010) Cadmium(II) sequestration characteristics by two isolates of *Synechocystis* sp. In terms of exopolysaccharide (EPS) production and monomer composition. *Bioresour. Technol.* **101**, 9742–9748.

Padan J., Marcinek S., Cindric A. M., Santinelli C., Broji S. R., Radakovitch O., Garnier C. and Omanovic D. (2021) Organic copper speciation by anodic stripping voltammetry in estuarine waters with high dissolved organic matter. *Front. Chem.* **8** 628749.

Paxeus N. and Wedborg M. (1985) Acid-base properties of aquatic fulvic acid. *Anal. Chim. Acta* **169**, 87–98.

Pedler-Sherwood B., Shaffer E. A., Reyes K., Longnecker K., Aluwihare L. I. and Azam F. (2015) Metabolic characterization of a model heterotrophic bacterium capable of significant chemical alteration of marine dissolved organic matter. *Mar. Chem.* **177**, 357–365.

Pernthaler J. (2005) Predation on prokaryotes in the water column and its ecological implications. *Nat. Rev. Microbiol.* **3**, 537–546.

Ritchie J. D. and Perdue E. M. (2008) Analytical constraints on acidic functional groups in humic substances. *Org. Geochem.* **39**, 783–799.

Saba G. K., Steinberg D. K. and Bronk D. A. (2011) The relative importance of sloppy feeding, excretion, and fecal pellet leaching in the release of dissolved carbon and nitrogen by *Acartia tonsa* copepods. *J. Exp. Mar. Biol. Ecol.* **404**, 47–56.

Saito M. A., Sigman D. M. and Morel F. M. M. (2003) The bioinorganic chemistry of the ancient ocean: the coevolution of cyanobacterial metal requirements and biogeochemical cycles at the Archean-Proterozoic boundary? *Inorg. Chim. Acta* **356**, 308–318.

Strom S. L., Benner R., Ziegler S. and Dagg M. J. (1997) Planktonic grazers are a potentially important source of marine dissolved organic carbon. *Limnol. Oceanogr.* **42**, 1364–1374.

Sunda W. G. and Huntsman S. A. (1995) Cobalt and zinc interreplacement in marine phytoplankton: biological and geochemical implications. *Limnol. Oceanogr.* **40**, 1404–1417.

Sunda W. G. (2012) Feedback interactions between trace metal nutrients and phytoplankton in the ocean. *Front. Microbiol.* **3**, 1–22.

Swaren L., Hao W., Melnyk S., Baker D., Li Y., Owttrim G. W., Zeng H., Gingras M. K., Alessi D. S. and Konhauser K. O. (2021) Surface reactivity of the cyanobacterium *Synechocystis* sp. PCC 6803 – Implications for trace metal transport to the ocean. *Chem. Geol.* **562** 120045.

Tremblay L., Caparros J., Leblanc K. and Obernosterer I. (2015) Origin and fate of particulate and dissolved organic matter in a naturally iron-fertilized region of the Southern Ocean. *Biogeosciences* **12**, 607–621.

Twining B. S. and Baines S. B. (2013) The trace metal composition of marine phytoplankton. *Annu. Rev. Mar. Sci.* **5**, 191–215.

Van den Berg C. M. G. and Nimmo M. (1987) Determination of interactions of nickel with dissolved organic material in seawater using cathodic stripping voltammetry. *Sci. Total Environ.* **60**, 185–195.

Vraspir J. M. and Butler A. (2009) Chemistry of marine ligands and siderophores. *Annu. Rev. Mari. Sci.* **1**, 43–63.

Walker B. D., Primeau F. W., Beaupre S. R., Guilderson T. P., Druffel E. R. M. and McCarthy M. D. (2016) Linked changes in marine dissolved organic carbon molecular size and radiocarbon age. *Geophys. Res. Lett.* **43**, 385–393.

Wang K., Wommack E. and Chen F. (2011) Abundance and distribution of *Synechococcus* spp. And cyanophages in the Chesapeake Bay. *Appl. Environ. Microbiol.* **77**, 7459–7468.

Waterbury J. B., Watson S. W., Guillard R. R. L. and Brand L. E. (1979) Widespread occurrence of a unicellular, marine, planktonic, cyanobacterium. *Nature* **277**, 293–294.

Worden A. Z., Nolan J. K. and Palenik B. (2004) Assessing the dynamics and ecology of marine picoplankton: the importance of the eukaryotic component. *Limnol. Oceanogr.* **49**, 168–179.

Yee N., Benning L. G., Phoenix V. R. and Ferris F. G. (2004) Characterization of metal-cyanobacteria sorption reactions; a combined macroscopic and infrared spectroscopic investigation. *Environ. Sci. Technol.* **38**, 775–782.

Yu Q., Szymanowski J., Myneni S. C. B. and Fein J. B. (2014) Characterization of sulfhydryl sites within bacterial cell

envelopes using selective site-blocking a potentiometric titrations. *Chem. Geol.* **373**, 50–58.

Zhang Y., Green N. W. and Perdue E. M. (2013) Acid-base properties of dissolved organic matter from pristine oil-impacted marshes of Barataria Bay, Louisiana. *Mar. Chem.* **155**, 42–49.

Zhang J., Kattner G. and Koch B. P. (2019) Interactions of trace elements and organic ligands in seawater and implications for quantifying biogeochemical dynamics: a review. *Earth-Sci. Rev.* **192**, 631–649.

Zhao Z., Gonsoir M., Luek J., Timko S., Ianiri H., Hertkorn N., Schmitt-Kopplin P., Fang X., Zeng Q., Jiao N. and Chen F. (2017) Picocyanobacteria and deep-ocean fluorescent dissolved organic matter share similar optical properties. *Nat. Commun.* **8**, 15284.

Zhao Z., Gonsoir M., Schmitt-Kopplin P., Zhan Y., Zhang J., Jiao N. and Chen F. (2019) Microbial transformation of virus-induced dissolved organic matter from picocyanobacteria: coupling of bacterial diversity and DOM chemodiversity. *ISME J.* **13**, 2551–2565.

Zheng Q., Chen Q., Cai R., He C., Guo W., Wang Y., Shi Q., Chen C. and Jiao N. (2019) Molecular characteristics of microbially mediated transformation of *Synechococcus*-derived dissolved organic matter as revealed by incubation experiments. *Environ. Microbiol.* **21**, 2533–2542.

Associate editor: Hailiang Dong